Validation Strategies for Satellite-Based Soil Moisture Products Over Argentine Pampas

Francisco Grings, Cintia A. Bruscantini, Ezequiel Smucler, Federico Carballo, María Eugenia Dillon, Estela Angela Collini, Mercedes Salvia, and Haydee Karszenbaum

***Abstract*—In this paper, an evaluation strategy for two-candidate satellite-derived SM products is presented. In particular, we analyze the performance of two candidate algorithms [soil moisture ocean salinity (SMOS)-based soil moisture (SM) and advanced scatterometer (ASCAT)-based SM] to monitor SM in Pampas Plain. The difficulties associated with commonly used evaluation techniques are addressed, and techniques that do not require ground-based observations are presented. In particular, we introduce comparisons with a land-surface model (GLDAS) and SM anomalies and triple collocation analyses. Then, we discuss the relevance of these analyses in the context of end-users requirements, and propose an extreme events-detection analysis based on anomalies of the standardized precipitation index (SPI) and satellite-based SM anomalies. The results show that: 1) both ASCAT and SMOS spatial anomalies data are able to reproduce the expected SM spatial patterns of the area; 2) both ASCAT and SMOS temporal anomalies are able to follow the measured *in situ* SM temporal anomalies; and 3) both products were able to monitor large SPI extremes at specific vegetation conditions.**

***Index Terms*—Cropland, passive microwaves, soil moisture, validation strategies.**

I. Introduction

SATELLITE-BASED soil moisture (SM) products are potentially useful for several key environmental applications (agro-meteorology, SM excess or deficit monitoring, etc.). The information provided by these systems is particularly relevant in Argentina's Pampas Plain, where *in situ* meteorological stations are scarce and frequent extreme environmental events strongly affect agricultural production.

There are several satellite-based, global, operational SM products available for the Pampas Plain area such as Aquarius sensor onboard SAC-D (NASA-CONAE mission) [1], advanced scatterometer (ASCAT) onboard METOP-A [2], MIRAS radiometer onboard the Soil Moisture Ocean Salinity (SMOS) Mission [3], advanced microwave scanning radiometer-earth observing system (AMSR-E) [4] and recently launched Soil Moisture Passive Active (SMAP) NASA Mission [5] (data not available yet). Nevertheless, SM products obtained from these satellite systems report different spatiotemporal patterns of SM for the same area and period of time. These products discrepancy was also observed for other areas around the world, and it is the subject of active research, since all these products claim some form of validation (in general, *in situ* validation in some densely instrumented sites), and were successfully used in several derived applications (e.g., assimilation in forecast models, SM-precipitation coupling, and run-off models). In some way, all existing products could represent "true" SM to some extent.

Therefore, it is relevant to ask which products best reproduce Pampas Plain SM spatiotemporal patterns. This is not an easy question to answer, since there are no validation sites in this area and therefore direct validation is not possible at the time. Therefore, since: 1) product quality in the area cannot be guaranteed by global validation and 2) direct *in situ* validation is not possible, alternative validation schemes become relevant.

In this paper, we analyze the performance of two-candidate algorithms (SMOS-based SM and ASCAT-based SM) to monitor SM in Pampas Plain. The selection of these two systems pretends to address passive and active instruments in view of future available data such as SMAP and Argentine SAOCOM missions [6]. In addition, a significant effort is done to introduce them as validated SM products. The difficulties associated with commonly used evaluation techniques based on the use of *in situ* networks are addressed, and techniques that do not require ground data are presented. In particular, we introduce comparisons with a land-surface model (GLDAS) and SM anomalies and triple collocation (TC) analyses [7]. Then, we discuss the relevance of these analyses in the context of end-users requirements, and propose an extreme events-detection analysis based on anomalies of the standardized precipitation index (SPI). Finally, the implications of these results to define site-specific operational evaluation strategies are discussed. The following sections address these subjects, starting with a short description of the Pampas Plains locations and of the characteristics of the satellite systems products under discussion.

II. Pampas Plains

Argentina's Pampas ($27-40°$S, $57-67°$W) is a wide plain of over 50 million ha of fertile lands suitable for cattle and crop

Manuscript received September 30, 2014; revised June 09, 2015; accepted June 11, 2015. Date of publication July 28, 2015; date of current version September 12, 2015. This work was supported in part by MinCyT-CONAE SAC-D/Aquarius project 12 and in part by the Inter-American Institute for Global Change Research (IAI) CRN 3035, which is supported by the U.S. National Science Foundation under Grant GEO-1128040.

F. Grings, C. A. Bruscantini, E. Smucler, F. Carballo, M. Salvia, and H. Karszenbaum are with the Quantitative Remote Sensing Group, Institute of Astronomy and Space Physics (IAFE), Consejo Nacional de Investigaciones Científicas y Técnicas (CONICET) and University of Buenos Aires, Buenos Aires 1428, Argentina (e-mail: verderis@iafe.uba.ar).

M. E. Dillon is with the Consejo Nacional de Investigaciones Científicas y Técnicas (CONICET) and Servicio Meteorológico Nacional (SMN), Buenos Aires C1022ABL, Argentina.

E. A. Collini is with the Servicio de Hidrografia Naval (SHN) and Servicio Meteorológico Nacional (SMN), Buenos Aires C1022ABL, Argentina.

Color versions of one or more of the figures in this paper are available online at http://ieeexplore.ieee.org.

Digital Object Identifier 10.1109/JSTARS.2015.2449237

production. Fig. 1 shows a land cover map of the area [8] and, as an example, the spatial distribution of the difference between precipitation (P) and evapotranspiration (EP) means (mm) of the period 1970–2006 for the month of October (growing season) as a reference of the hydrological characteristics of the area, drier in the west and wetter in the east [9]. Most of the Pampas region are significantly affected by cyclical drought and flood episodes that impact both crop and cattle production [10].

III. Available Data

A. Satellite Data

There are several satellite-based SM products available in the study area. For this study, we selected two of them (ASCAT and SMOS) whose overall global performance and the fact that are widely used makes them candidates to provide a reasonable estimation of SM spatiotemporal distribution in our study area. The different evaluation strategies presented in this paper used different subsets of SM measurements of the period 2010–2014.

The SMOS satellite was launched in 2009 and is dedicated to SM retrieval at $\sim 5\ \mathrm{cm}$ depth using brightness temperature measured at L-band (passive microwave, ground resolution $\sim 25\ \mathrm{km}$). It has a single observation frequency (1.4 GHz), but uses observations at multiple incident angles. The standard SMOS algorithm is based on the L-MEB (L-band microwave emission of the biosphere) model and it adopts a forward modeling approach to solve for SM [3]. In this paper, we used the SM data set provided by EOLI-SA data source.

The ASCAT sensor onboard the MetOp-A measures the backscattering coefficient at C-band and at multiple incidence angles (active microwave, ground resolution $\sim 25\ \mathrm{km}$). The SM estimation is obtained using a time-series-based change-detection algorithm [2]. Since the SM changes can be measured in relative terms, the estimation becomes less susceptible to the adverse influence of vegetation cover and surface roughness, although it should be noted that active sensors are more susceptible to roughness and vegetation than passive sensors.

Regarding the performance of SMOS and ASCAT SM, from a theoretical point of view, it is expected that SMOS SM product (which uses L-band data) should be less affected by vegetation. On the contrary, ASCAT SM product (active C-band) should present more vegetation contamination.

B. LSM Data

Other relevant providers of SM spatiotemporal distribution information are land-surface models (LSMs). These models estimate SM solving the energy/mass balance in the earth surface and constraints its retrieval assimilating *in situ* data. In order to compare models and product estimations, we included in the present analysis the first layer SM field from the NOAH LSM model, one of the models available from the GLDAS version 2.0 data set (12 h GMT). GLDAS SM product is produced by specific instances of the land information system (LIS) software framework for high-performance land-surface modeling and data assimilation developed within the Hydrological Sciences Laboratory at NASA Goddard [11], [12]. This version of GLDAS uses as forcing data the one provided by Princeton University [13].

In order to quantitatively analyze the data, products were gridded into the GLDAS official grid of 0.25° resolution using nearest-neighbor interpolation.

C. In Situ Data

Although no field validation site exists in the study area, there are SM data available (one point), acquired in the SOL NEGRO agricultural site near the city of Cordoba, Argentina. SM was measured using an Hydra Probe II system with a sampling depth of 5 cm every hour since September 2012 [14].

Since point SM measurements provide only spatially limited validation capacity, we estimated soil hydrological condition using the SPI. Therefore, *in situ* precipitation data were extensively used. Over the area considered, the National Meteorological Service (NMS) of Argentina provides daily precipitation data of approximately 50 ground stations.

IV. Methodology

A. Spatial Anomalies

As we will see in the following section, due to the limited availability of *in situ* data in this region in terms of spatial distribution, period covered, and quality control yet to be established, a direct comparison between SM products leads to poor results both quantitatively and qualitatively, since it does not allow answering the questions posed in Section I. Therefore, in order to compare the spatial patterns of the three SM data sets, we generated maps of each of the products' standardized spatial anomalies [7]. For each SM data set, standardized spatial anomalies were calculated in three steps, as follows. We first calculated the product's temporal mean for each grid point in the study region. Second, we calculated the spatial mean and standard deviation of the means calculated in the first step. Finally, we defined the standardized spatial anomaly of the given SM data set at a given grid point as the difference between the mean calculated at that grid point in the first step and the spatial mean calculated in the second step, divided by the spatial standard deviation calculated in the second step. These maps provide information on how similarly each of the SM data sets represents wet/dry conditions over the study region. In order to quantify this information, we calculated the linear correlation coefficient between the standardized spatial anomalies of each pair of SM data sets [7].

B. Triple Collocation (TC)

The triple collocation (TC) technique, developed by Stoffelen [15], is a tool to estimate the root-mean-squared error (RMSE) with respect to the real *in situ* variable in remote sensing products. This technique is used here to estimate RMSE of the SM anomalies time series generated by GLDAS (X), SMOS (Y), and ASCAT (Z) [16]. The SM temporal anomalies time series were defined as the deviations of the original time series from their seasonal climatology. For each data set, the seasonal climatology was calculated as the 31 day moving average, where the averages are based on data from the whole

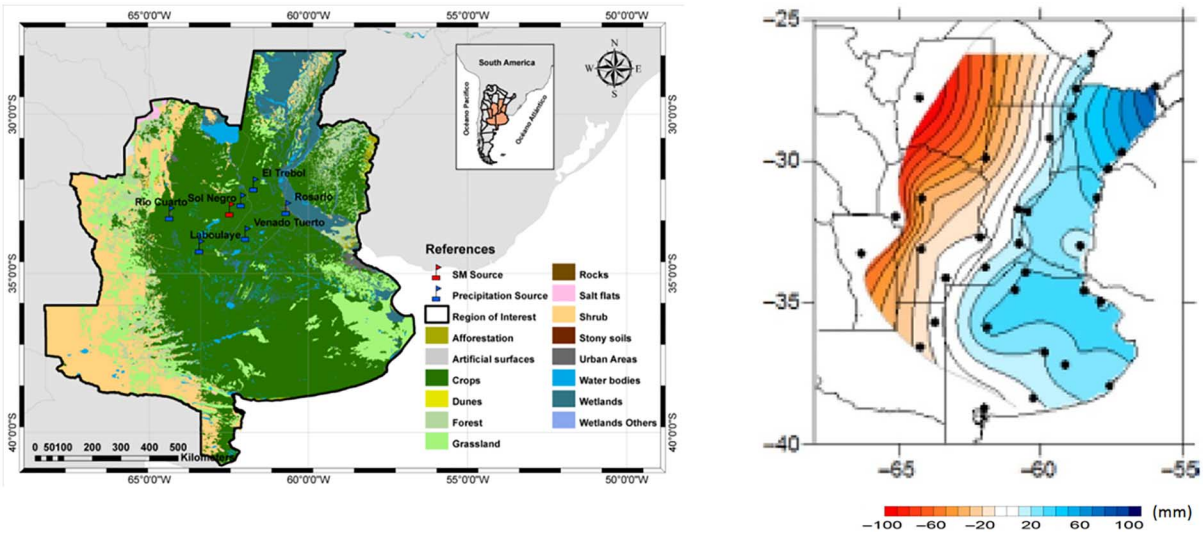

Fig. 1. Study area. *Left*: Pampas Plains land cover categories (2006–2009 period, 1:500 000 scale) (adapted from [8]). *Right*: An example of the spatial distribution of the P-EP means (mm) for the period 1970–2006 for the month of October (adapted from [9]).

period of study for the 31 day window surrounding each day of the year.

At each grid point and for each data set, TC adopts the following model to relate the data sets to the (unknown) true SM anomalies (t)

$$X = \beta_X(t + \varepsilon_X) \tag{1}$$

$$Y = \beta_Y(t + \varepsilon_Y) \tag{2}$$

$$Z = \beta_Z(t + \varepsilon_Z) \tag{3}$$

where β_i and ε_i for $i = \mathrm{X}, \mathrm{Y}, \mathrm{Z}$ are the TC calibration constants and errors corresponding to GLDAS, SMOS, and ASCAT, respectively. The errors ε_i for $i = \mathrm{X}, \mathrm{Y}, \mathrm{Z}$ are assumed to be zero-mean random variables, which are uncorrelated with each other and with the truth (t). The calibration constants are used to rescale the data sets, so as to eliminate systematic differences in their variability. Since (1)–(3) are underdetermined, one data set is chosen as the reference and the other two are rescaled to the reference time series. The data set chosen as the reference here is GLDAS. This selection is not arbitrary, since we expect GLDAS to provide the SM benchmark information for the area.

Therefore, we set $\beta_X = 1$ and estimate the remaining calibration constants via

$$\beta_Y = \frac{< YZ >}{< XZ >}$$

$$\beta_Z = \frac{< YZ >}{< XY >}.$$

Here, $< >$ stands for a long-term average. Finally, we obtain the TC estimates of the variances of ε_i, $i = \mathrm{X}, \mathrm{Y}, \mathrm{Z}$, which we note, $Var_{TC}(\varepsilon_i)$, from

$$Var_{TC}(\varepsilon_X) = \left\langle \left(X - \frac{Y}{\beta_Y}\right)\left(X - \frac{Z}{\beta_Z}\right)\right\rangle$$

$$Var_{TC}(\varepsilon_Y) = \left\langle \left(\frac{Y}{\beta_Y} - X\right)\left(\frac{Y}{\beta_Y} - \frac{Z}{\beta_Z}\right)\right\rangle$$

$$Var_{TC}(\varepsilon_Z) = \left\langle \left(\frac{Z}{\beta_Z} - X\right)\left(\frac{Z}{\beta_Z} - \frac{Y}{\beta_Y}\right)\right\rangle.$$

The square root of the estimated error variances is the TC estimates of the RMSE. Since GLDAS was taken as the reference data set, all estimates are given in GLDAS climatology, but they can be easily converted to another reference data set by multiplying with the appropriate calibration constant.

It should be noted that in order for these estimates to be consistent, all the assumptions of the TC error model should hold. This is the case for the data sets used in this study, since no two of them use common input data or observations that could produce significantly correlated errors. Finally, it is important to remark that since the TC study is based on deviations from the mean seasonal cycle, the estimates obtained represent only the errors in the anomalies of the SM time series, and therefore, they do not provide any insight into errors in the mean season cycle or bias in the original time series.

C. Standardized Precipitation Index (SPI) and Extremes Definition

The standardized precipitation index (SPI) was designed by McKee *et al.* [17] to monitor the water supply conditions of a particular region. Its simplicity and versatility are given by its dependence with only one variable, the precipitation, and the possibility to be calculated on any timescale. Moreover, the frequencies of the extreme and severe droughts classifications for any location and timescale are consistent [18]. In this paper, SPI is computed monthly, and following the classification proposed by McKee *et al.* [17], an hydrological extreme in an area is considered if Abs(SPI) > 2.

Therefore, we decided to use the SPI as an objective measurement of precipitation anomalies to define extreme conditions of water supply during the analyzed period. The NMS of Argentina operationally provides this index for different scales, considering the precipitation distribution of 1961–2000 as the reference interval (refer to http://www.smn.gov.ar/serviciosclimaticos/). The SPI categories scale is detailed in Figs. 7–11 of Section V.

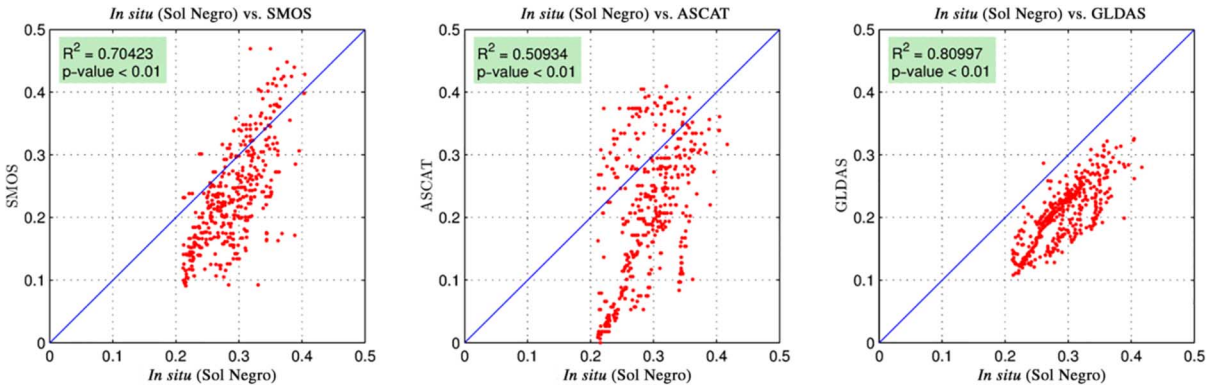

Fig. 2. Direct comparison among SMOS, ASCAT, and GLDAS SM estimations and *in situ* SM measurements (January 2010–December 2012).

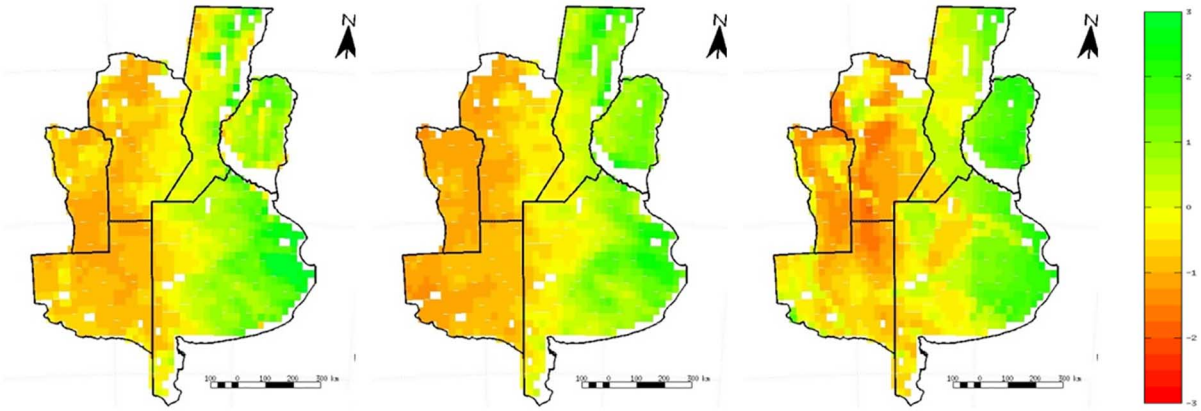

Fig. 3. Product spatial anomalies of SMOS, ASCAT, and GLDAS SM values (Austral Winter June 2010–September 2010).

V. Results

A. Preliminary Analysis

As a preliminary analysis, we checked the consistency between product SM values and available *in situ* data. Although *in situ* data consist of only one point and therefore has limited representativeness, this first check is relevant to delineate the following operational evaluations strategies. Results are shown in Fig. 2.

From the data, we can see that: 1) the correlation of SMOS and GLDAS with *in situ* data is relatively high, while the same correlation for ASCAT is relatively low; 2) both SMOS and ASCAT present larger dynamic ranges than *in situ* data ($0.4\,\mathrm{g/g}$ versus $0.2\,\mathrm{g/g}$ for *in situ* data); 3) satellite products present different maximums and minimums (SMOS $0.1 - 0.5$ g/g, ASCAT $0 - 0.4$ g/g); and 4) GLDAS present only a systematic underestimation, which seems to be constant along all the SM ranges.

From these observations, we can extract two preliminary results of our study area. First, GLDAS seems to be a good SM benchmark for this area (except or a systematic bias) and second, a comparison of absolute values of SM is not a convenient way to analyze satellite product performance, since products and *in situ* data in this region present different dynamic ranges, maximums and minimums.

B. Spatial Anomalies Analysis

Since absolute SM estimations of satellite products presented a low performance when compared to *in situ* SM data, it is relevant to compute SM spatial anomalies estimations as defined in Section IV-A. Anomalies so defined have the potential to follow *in situ* SM anomalies, which can be very useful to several end-user applications. Fig. 3 shows an example of Austral Winter standardized spatial anomalies for both products and GLDAS for the 2010 period.

TABLE I
Correlation Between Product Anomalies

	Correlation	p-Value
SMOS vs. ASCAT	0.879	< 0.01
ASCAT vs. GLDAS	0.789	< 0.01
SMOS vs. GLDAS	0.772	< 0.01

As seen, although the performance of absolute values is low, all spatial anomalies present high correlation among them (see Table I). More important, spatial anomalies present the typical east–west SM gradient of the study area. This indicates that although satellite products and GLDAS present different dynamic ranges and sensitivities, they all carry some information about Pampas Plain SM spatial pattern. Moreover, this information is consistent with the available macro-meteorological information, which is specifically modeled by GLDAS and reproduced (to some degree) by satellite-based products. This correlation between products and LSM (second and third row of Table I) is particularly relevant, since satellite-based products do not take any meteorological data as input.

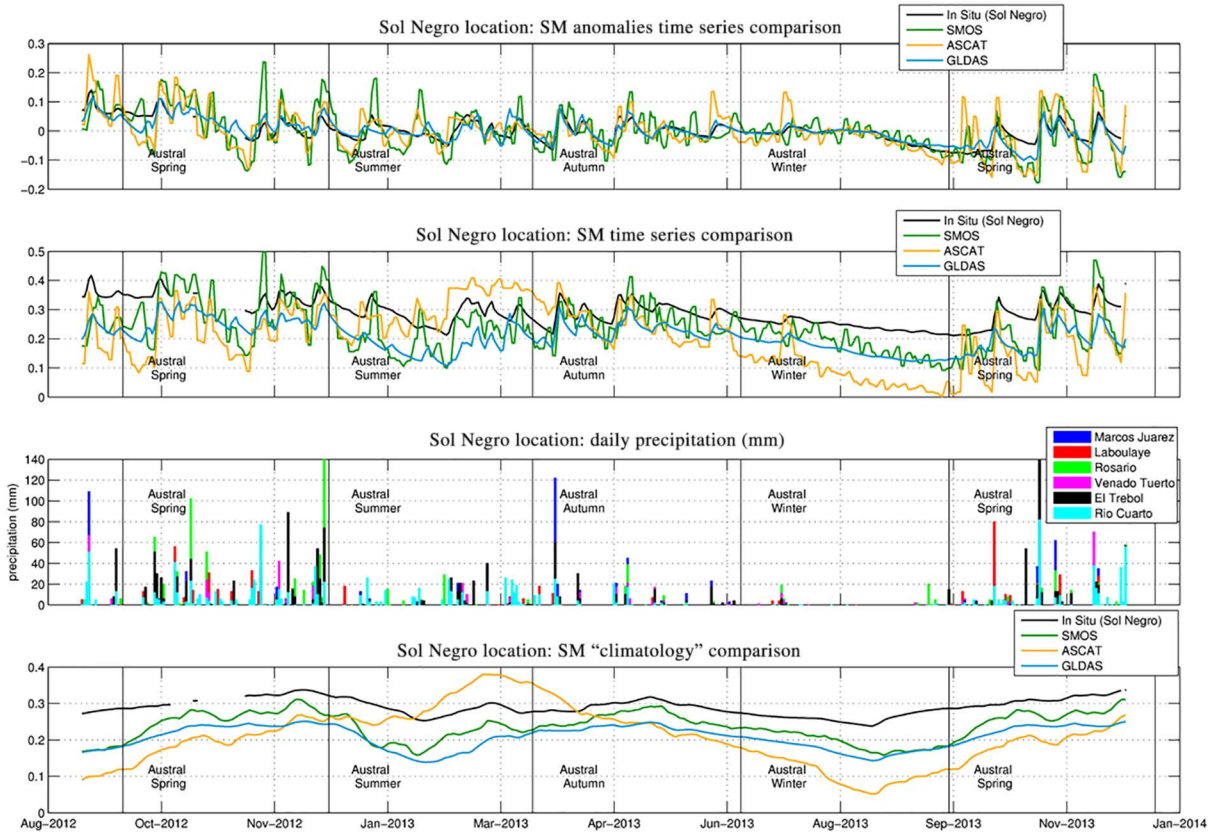

Fig. 4. SM temporal anomalies in the first row. SM absolute values in the second row. Precipitation stations close to Sol Negro site in the third row. Climatology for SMOS, ASCAT, GLDAS, and *in situ* measurements in the fourth row. The period was constrained to the time period where *in situ* measurements were available (September 12–January 14).

C. Temporal Anomalies Analysis

The behavior of the temporal anomalies as defined in Section IV-B in the site in which *in situ* SM data are available is presented in Fig. 4.

As seen, in the only site where comparisons with *in situ* measurements were possible, the temporal trend of SM temporal anomalies in general follows *in situ* measurements (first row). Moreover, SM temporal anomalies are sensitive to major precipitation events in the area (third row). On the contrary, absolute SM values present medium to large deviations from *in situ* measurements. The reasons of these deviations can be several, and complex, with strong underestimations and overestimations for all the SM products analyzed. Nevertheless, we believe that a clue is provided by the temporal behavior of the climatology. *In situ* SM climatology presents low annual variations for this area, while ASCAT satellite product climatology presents strong annual variations, with minimums in winter and maximums in summer.

In summary, absolute satellite-based SM estimation presents strong discrepancies (dynamic ranges, variability, sensitivity to precipitations, seasonal behavior, and others) among them and with *in situ* measurements. Nevertheless, SM spatial anomalies are quite similar (they show good correlation among them) and therefore worthy of being analyzed using an advanced technique as TC.

D. TC Analysis

TC is able to estimate the error between real SM anomalies and satellite SM anomalies, given a triplet of SM anomalies. TC results are summarized in Fig. 5 and Table II. Fig. 5 shows three maps of the TC error estimations for each pixel and each product. As seen, ASCAT and SMOS present similar spatial distributions of overall TC errors, while GLDAS present more spatially homogeneous results. Larger errors in ASCAT seem to be located in areas of large biomass (crops), while SMOS errors are mainly located in coastal areas.

Table II summarizes the main statistics of the TC analysis. It can be seen that the mean value of the error is very similar for all the three products for this area and the time period analyzed. This implies that the error between true SM anomalies and SMOS and ASCAT SM anomalies are similar. These results can be further visualized in Fig. 6.

Fig. 6 shows a map of the satellite product that presents the lower TC error estimate. A pixel is assigned to a given product if $\mathrm{TC}_1 - \mathrm{TC}_2 >$ threshold, where the threshold was selected as 0.002. As seen in the figure, the vast majority of the area is labeled as "Tie," indicating very similar TC error estimates for both products and also very similar errors between true SM anomalies and satellite SM anomalies.

From this analysis, it can be seen that the mean value of the TC error is very similar for all the products. Moreover,

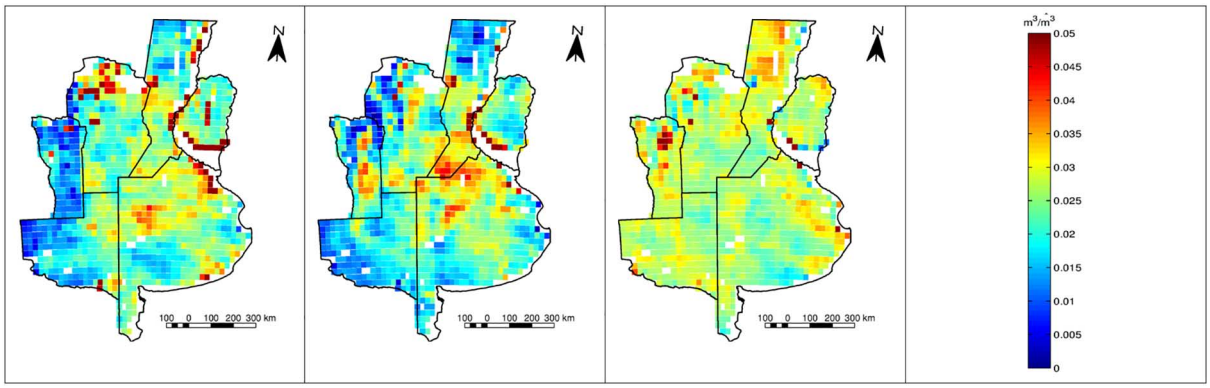

Fig. 5. Overall TC error estimation for SMOS, ASCAT, and GLDAS.

TABLE II
MEAN, MEDIAN, AND SD OF OVERALL TC ESTIMATES

	GLDAS	ASCAT	SMOS
Mean	0.0273	0.0238	0.0270
Median	0.0268	0.0221	0.0231
SD	0.0052	0.0226	0.0473

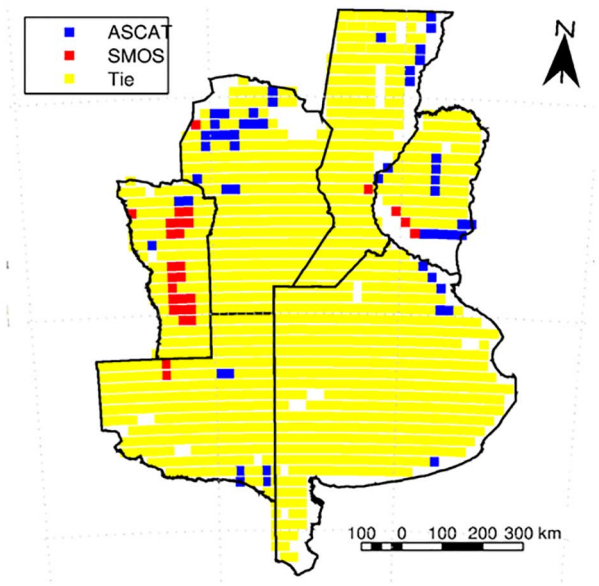

Fig. 6. Map of the product which presents the minimum TC error estimation (errors are considered the same if $\mathrm{TC}_1 - \mathrm{TC}_2 > 0.002$).

repeating this analysis for different time periods, seasons, and land cover selections produce different results of TC error estimates (results not shown), with no definite best product. Therefore, if we seek an answer to which product best represents spatiotemporal SM patterns in this area and time period, TC analysis does not provide a conclusive answer.

Since standard metrics (anomalies analysis and TC error estimation) produce positive but inconclusive evidence, to evaluate product performance, we propose an extreme event-detection analysis based on anomalies of the SPI.

E. SPI Extreme Events Analysis

SPI is commonly used as an excess/shortage soil water indicator in areas where precipitation data are available, although *in situ* SM data may not be available. As stated in the methodology, SPI is computed monthly. The methodology proposed is based on the analysis of the extremes defined by SPI. We defined an hydrological extreme in an area if $\mathrm{Abs}(\mathrm{SPI}) > 2$. This operational definition has two advantages. First, although the real values of SM and SPI are not generally correlated, when such an extreme conditions exist, extremes values of SM are generally observed [18]. Second, this definition has the added value of being closely related to several end-user requirements, which are mainly interested in extreme events associated with extremes in precipitation.

Before proceeding with the analysis, it is relevant to address the expected SM spatial structure of the events, since by definition, SPI extremes are relatively large (of the order of 10^6 ha). At these spatial scales, positive extremes does not imply uniformly wetter areas, since in this flat plain, the water enters the system mainly by precipitation, which is spatially heterogeneous [19]. This implies that a positive extreme will be seen as an increase in SM values, but not necessarily a significant increase in mean SM values. On the contrary, negative extremes, characterized by the uninterrupted reduction of precipitation, will be more spatially homogeneous, since the main forcing that extracts water from the system is the evapotranspiration, which at these scales depends mainly on Sun's total irradiation.

Using these definitions, five extreme events were identified in the 4-year time series. These events as seen by the SPI and the SM values for the whole time series minus the extreme month (left boxplot), and the extreme month for the area of the event (right boxplot) for GLDAS, ASCAT, and SMOS are presented in Figs. 7–11. Each event will be analyzed independently.

1) Event #1: April 2010 (Fig. 7): The lack of sensitivity for this particular event can be related to several facts other than product performance. First, the event is spatially small, which is usually related to relatively large errors related to precipitation interpolation. Second, in April (Austral Autumn), main crop (soybean) is at its maximum biomass. Therefore, vegetation

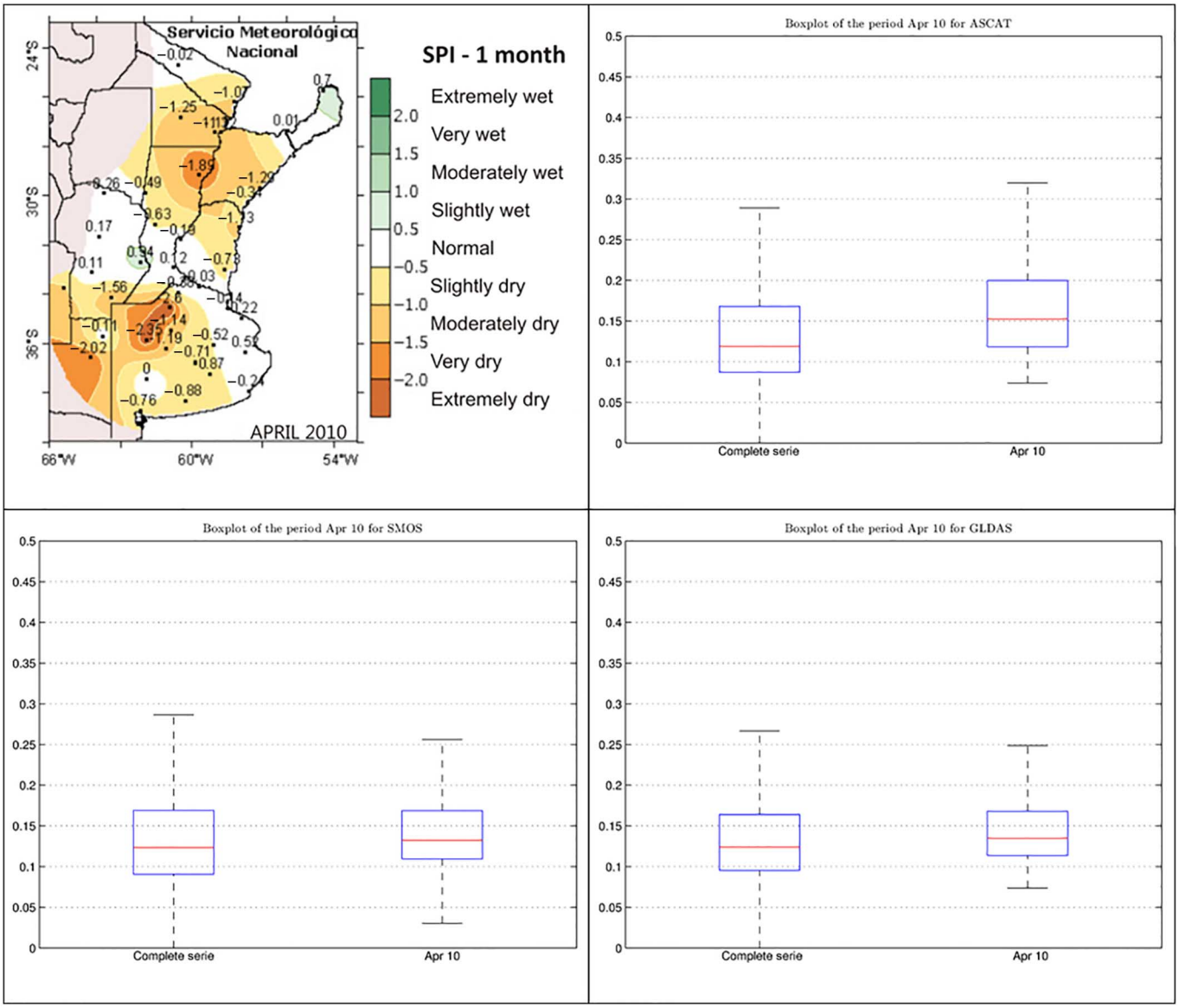

Fig. 7. SPI anomalies as seen by SPI, ASCAT, SMOS, and GLDAS. April 2010 event.

attenuation correction of satellite-based estimations is critical in this period of the year.

2) Event #2: January 2011 (Fig. 8): Wet anomaly: Significant increases are observed between the boxplots of the event compared to the one of the complete time series for ASCAT (median from 0.12 to $0.15\ \mathrm{m}^3/\mathrm{m}^3$, third quartile from 0.17 to $0.24\ \mathrm{m}^3/\mathrm{m}^3$, and upper whisker from 0.31 to 0.42 $0.42\ \mathrm{m}^3/\mathrm{m}^3$). No significant differences are observed for GLDAS and SMOS.

The event is medium-sized and occurred during Austral Summer (relatively high biomass). Boxplots show that some pixels inside the area show an increase in SM values, which corresponds to more heterogeneous SM values inside the area of the event. This is consistent with the expected behavior of the SM spatial pattern during a wet event as explained before.

3) Event #3: December 2011 (Fig. 9): Dry anomaly: Significant reductions are observed between the boxplots of the event compared to the one of the complete time series for all the products (median from 0.17 to 0.11 $0.11\ \mathrm{m}^3/\mathrm{m}^3$ in GLDAS, from 0.17 to 0.10 $0.10\ \mathrm{m}^3/\mathrm{m}^3$ in ASCAT, and from 0.16 to $0.009\ \mathrm{m}^3/\mathrm{m}^3$) in SMOS. Similar decreases are observed in the first and third quartile and upper whiskers for all products.

This event has a large size and occurred during Austral Summer (relatively high biomass). Boxplots show that the majority of pixels inside the area decrease their SM values, which corresponds to a less heterogeneous SM values inside the area of the event. This is consistent with the expected behavior of the SM spatial pattern during a dry event as explained before.

4) Event #4: February 2012 (Fig. 10): Wet anomaly: No significant differences are observed between the boxplots of the event compared to the one of the complete time series.

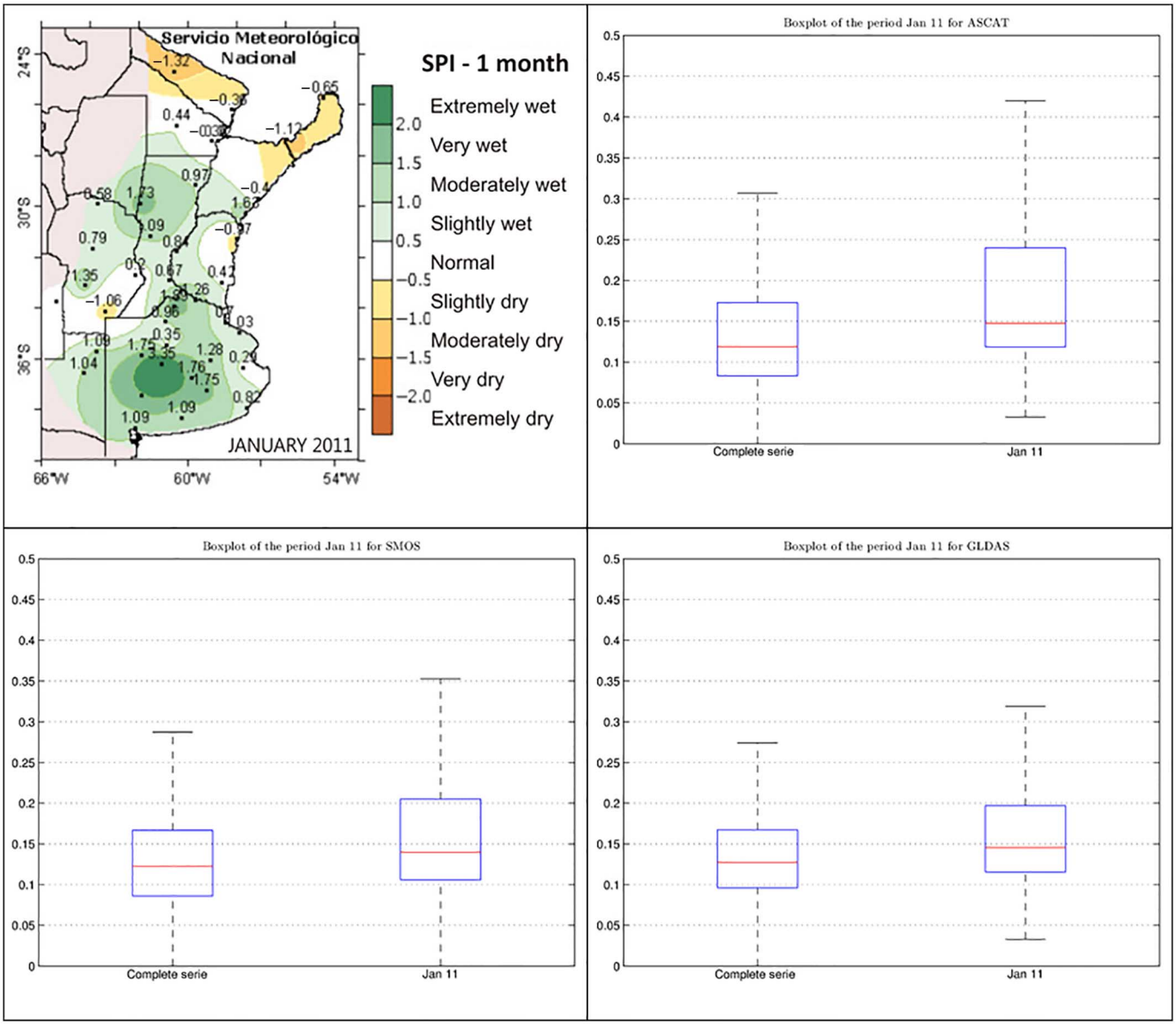

Fig. 8. SPI anomalies as seen by SPI, ASCAT, SMOS, and GLDAS. January 2011 event.

This event corresponds to two spatially disjoint events. The east event is located over Parana River Delta, for which SM estimations are not available (flagged in the products). Finally, the event occurs in Austral Summer (high biomass).

5) Event #5: August 2012 (Fig. 11): Wet anomaly: Significant increases are observed between the boxplots of the event compared to the one of the complete time series for all the products (median, third quartile, and upper whiskers).

This event has a large size and occurs in Austral Winter (low values of biomass). Boxplots show several pixels that increased their SM values, which correspond to more heterogeneous SM values inside the area of the event. This is consistent with the expected behavior of the SM spatial pattern during a wet event as explained before.

VI. Discussion

In this paper, a first analysis of the performance of two-candidate SM products (ASCAT and SMOS) over Argentine Pampas Plain was presented. The overall performance metric was defined as the ability to monitor SM spatiotemporal patterns. Since product absolute SM values presented large discrepancies, our approach to measure this ability consisted in using four different metrics: 1) SM spatial anomalies analysis; 2) SM temporal anomalies analysis; 3) TC error estimation analysis; and 4) SPI extreme events analysis.

A. SM Spatial Anomalies Analysis

Spatial anomalies analysis was overall successful, since it showed that both satellite-based products and GLDAS were

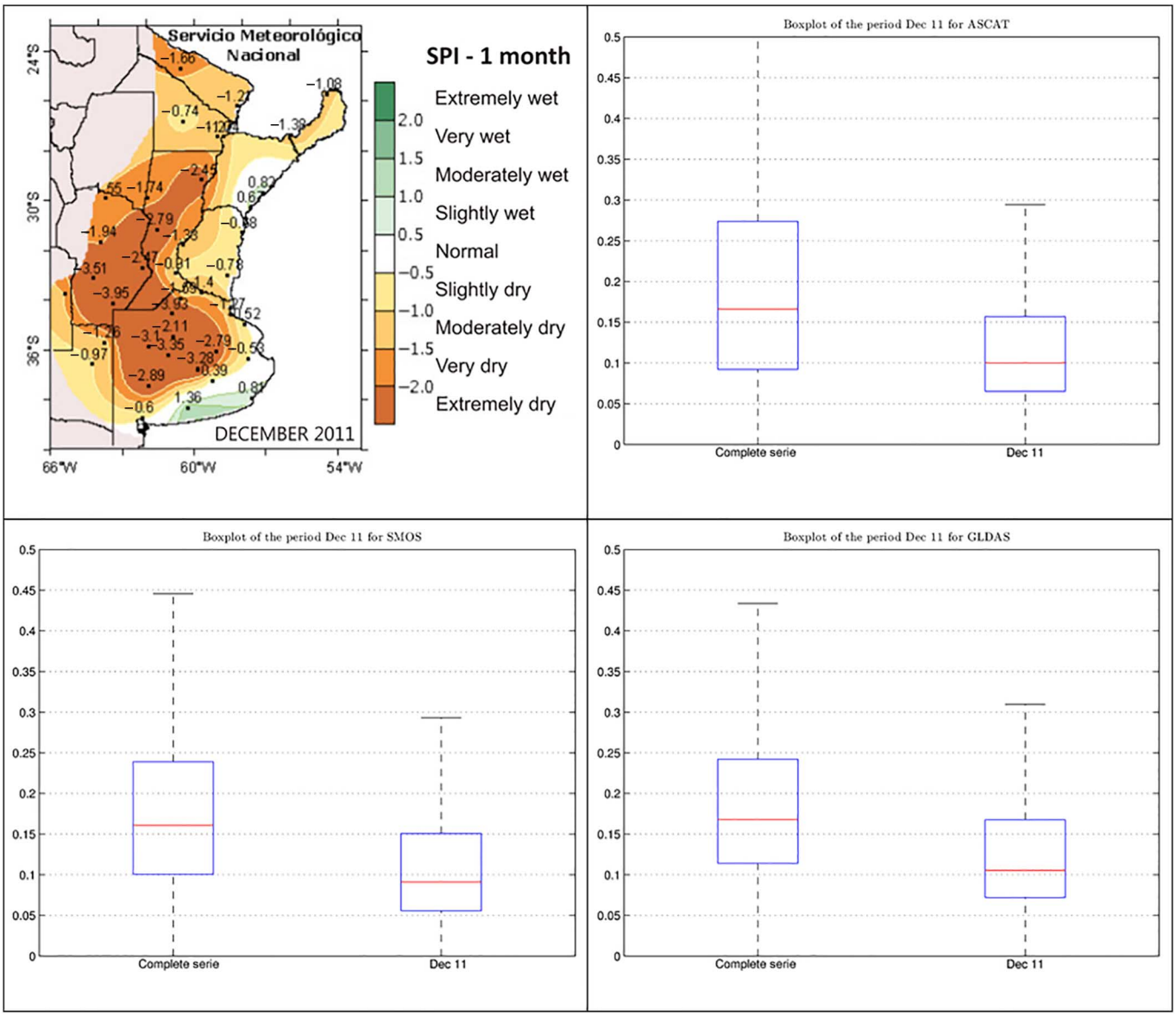

Fig. 9. SPI anomalies as seen by SPI, ASCAT, SMOS, and GLDAS. December 2011 event.

able to reproduce similar large-scale macro-meteorological SM patterns in the study area. This is observed in good correlation among anomalies (Table I) and in similarities between products and GLDAS. The satellite-derived spatial anomalies present the typical east–west SM gradient of the study area, which is related to specific precipitation and evapotranspiration patterns (see Fig. 1, *right*). This indicates that satellite products carry valuable information about overall Pampas Plain SM spatial pattern. This correlation between products and expected SM patterns is important, since satellite-based products do not take precipitation or evapotranspiration data as input.

B. SM Temporal Anomalies Analysis

It is relevant to mention that *in situ* SM climatology presented low annual variations for Sol Negro Station (*in situ* SM available), while ASCAT satellite product climatology presented strong annual variations, with minimums in winter and maximums in summer. Although there is no sufficient evidence to test this hypothesis, it is probable that this artifact is related to incomplete vegetation attenuation correction due to C-band limitations. Given the amount and quality of data available, no further interpretation can be provided.

C. TC Error Estimation Analysis

From the TC analysis, it was possible to generate a map of the overall TC error estimations for the study area (Fig. 5). These results were summarized in Table II. In general terms, larger errors in ASCAT seem to be located in the areas of large biomass (crops), while SMOS errors are mainly located in the coastal areas. The first also seem to be related to incomplete vegetation attenuation correction, which is particularly

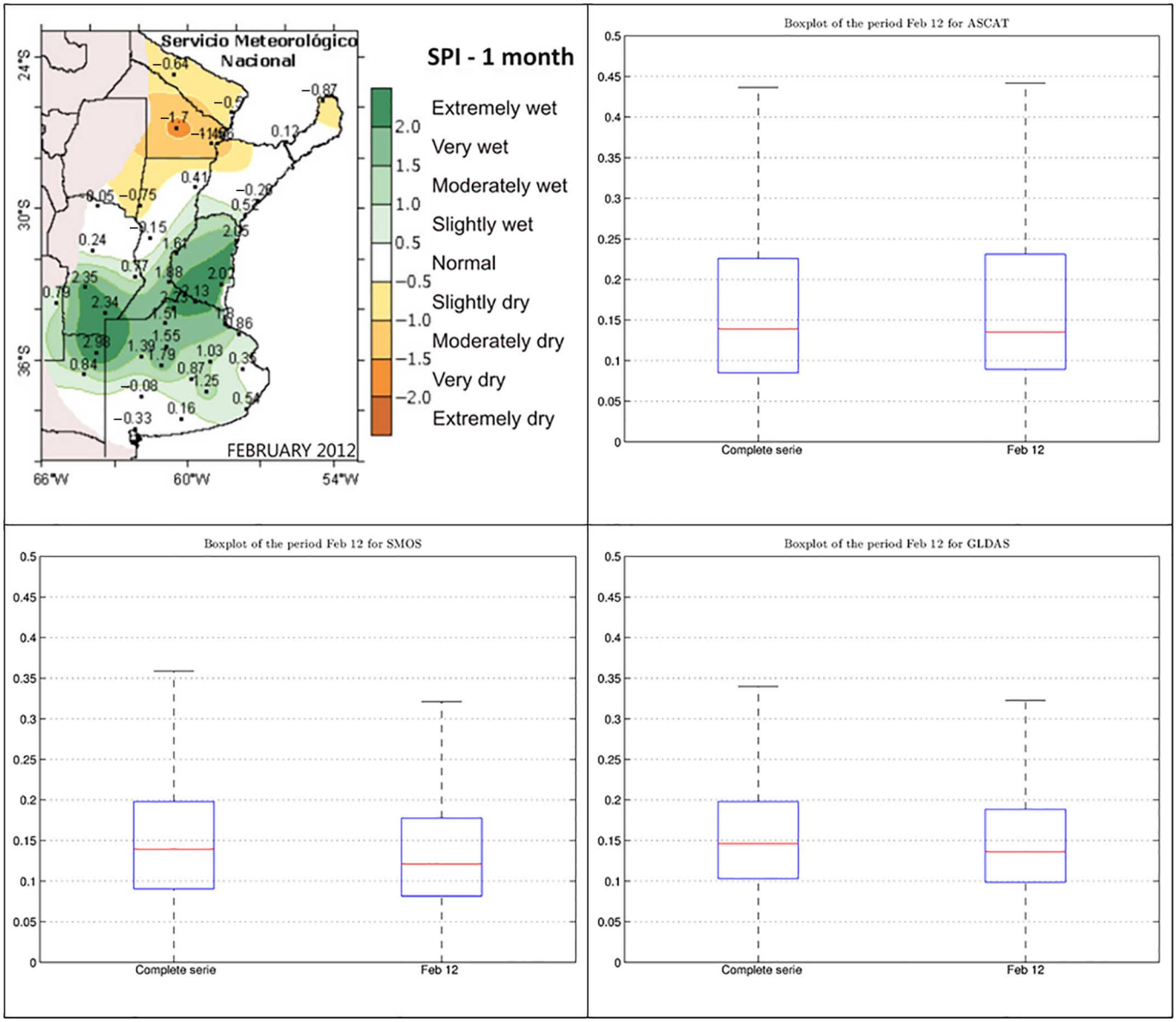

Fig. 10. SPI anomalies as seen by SPI, ASCAT, SMOS, and GLDAS. February 2012 event.

relevant at C-band, while the second could be related to: 1) geolocation errors associated with SMOS data generation strategy [3] or 2-D image reconstruction algorithm being affected by mixed-pixels with abrupt transitions. Nevertheless, considering a minimal error difference as significant, in most of the study area, the products are characterized by the same TC error estimates (see Fig. 6).

D. SPI Extreme Events Analysis

Extreme results are probably the most relevant result of this paper. In this analysis, it was shown that products are able to follow some SPI extremes (ASCAT: 3 of 5; SMOS: 2 of 5) present in the 4-year time series available. For the extremes that were not detected, several explanations were presented. First, arguments related to SPI overall quality for small areas, in which spatial interpolation of precipitation is critical, were discussed (event #1). Second, considerations about seasonality were discussed in the context of vegetation biomass. Indeed, vegetation attenuation correction is the main issue of several satellite-based SM products. Since Pampas Plain is a cropland, vegetation cycle of the area are synchronous and peaks at Austral summer, leading to larger biomass, larger attenuations, and more important corrections. Due to operational wavelength and physical constraints, this correction can be the key factor that controls product performance. This is, therefore, more important at C-band (ASCAT) than at L-band (SMOS).

In summary, satellite-based products were able to follow extreme hydrological events when biomass was low and more homogeneous (Austral winter, event #5) or biomass was moderate to high but the event was strong and spatially large (events #2 and #3).

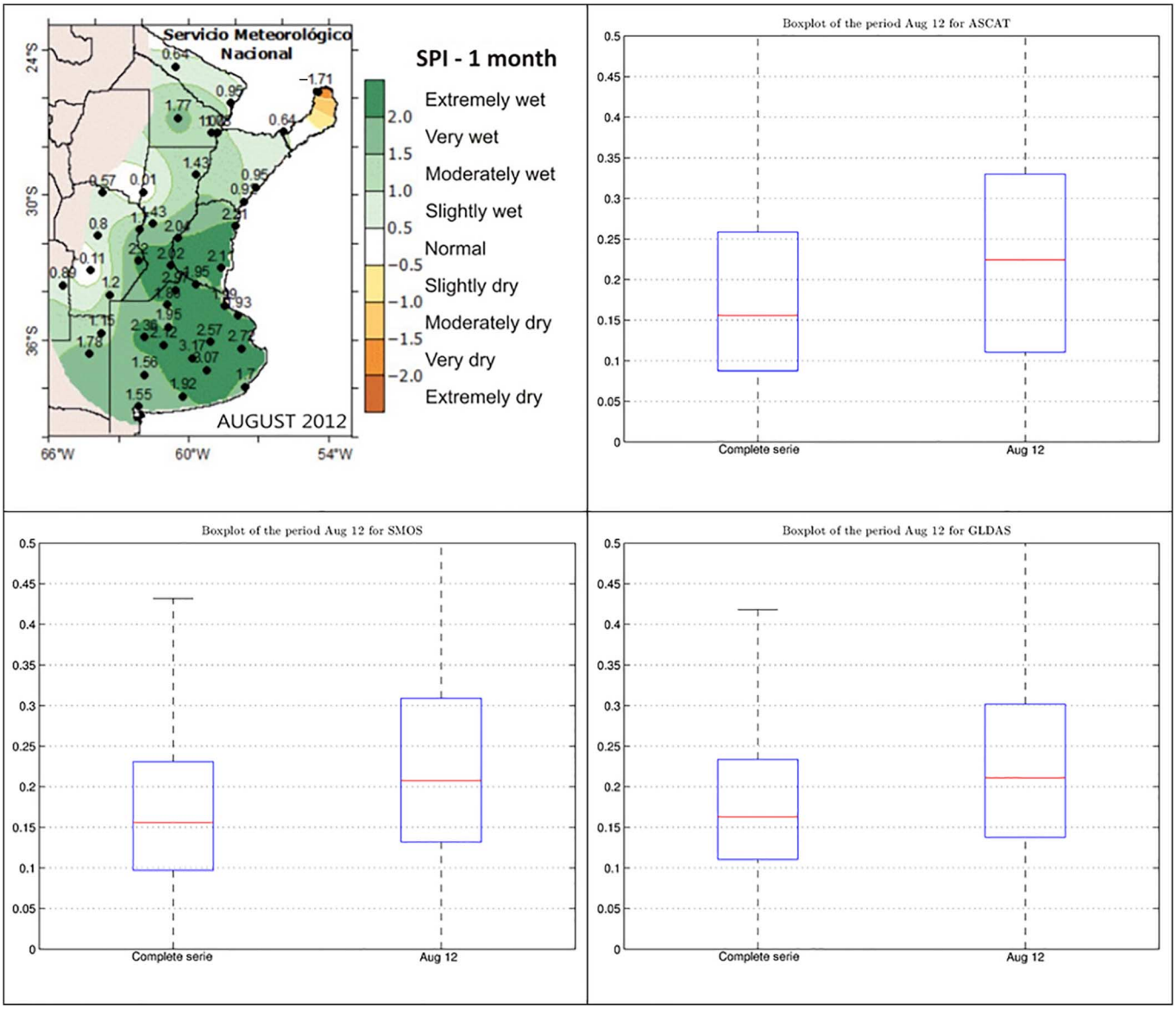

Fig. 11. SPI anomalies as seen by SPI, ASCAT, SMOS, and GLDAS. August 2012 event.

VII. Conclusion

In this paper, an evaluation strategy for two-candidate satellite-derived SM products was presented. The strategy involves only the analysis of data, which are satellite-derived or common in most areas (like precipitations). It is an evaluation and not a validation, since no *in situ* field experiment of the required size and instrumentation is available in the area, and therefore no proper validation is possible. On the contrary, the proposed methodology relies in comparison of product SM metrics that show expected SM spatiotemporal patterns. These metrics were selected to overcome product limitations, and to be able to provide relevant information to the end user. In this context, it was shown that: 1) both ASCAT and SMOS spatial anomalies data are able to reproduce the expected SM spatial patterns; 2) both ASCAT and SMOS temporal anomalies are able to follow the measured *in situ* SM temporal anomalies; and 3) both products were able to monitor large SPI extremes, at least in conditions where crop biomass was moderate to low.

Acknowledgment

The authors would like to specially thank Dr. W. Crow for the triple collocation code and CONAE for *in situ* SM data.

References

[1] D. M. Le Vine, G. S. E. Lagerloef, and S. E. Torrusio, "Aquarius and remote sensing of sea surface salinity from space," *Proc. IEEE*, vol. 98, no. 5, pp. 688–703, May 2010, doi: 10.1109/JPROC.2010.2040550.

[2] W. Wagner *et al.*, "The ASCAT soil moisture product: A review of its specifications, validation results, and emerging applications," *Meteorologische Zeitschrift*, vol. 22, no. 1, pp. 5–33, 2013.

[3] Y. H. Kerr *et al.*, "The SMOS soil moisture retrieval algorithm," *IEEE Trans. Geosci. Remote Sens.*, vol. 50, no. 5, pp. 1384–1403, May 2012.

[4] E. G. Njoku, *AMSR-E/Aqua L2B Surface Soil Moisture, Ancillary Parms, & QC EASE-Grids. Version 2*. Boulder, CO, USA: NASA National Snow and Ice Data Center Distributed Active Archive Center, 2004, doi: 10.5067/AMSR-E/AE_LAND.002.

[5] D. Entekhabi *et al.*, "The soil moisture active passive (SMAP) mission," *Proc. IEEE*, vol. 98, no. 5, pp. 704–716, 2010.

[6] D. D'Aria, D. Giudici, A. M. Guarnieri, P. Rizzoli, and J. Medina, "A wide swath, full polarimetric, L band spaceborne SAR," in *Proc. IEEE Radar Conf. (RADAR'08)*, May 26–30, 2008, pp. 1–4, doi: 10.1109/RADAR.2008.4720789.
[7] C. R. Hain, W. T. Crow, J. R. Mecikalski, M. C. Anderson, and T. Holmes, "An intercomparison of available soil moisture estimates from thermal infrared and passive microwave remote sensing and land surface modeling," *J. Geophys. Res.*, vol. 116, pp. 1–18, 2012.
[8] INTA (Instituto Nacional de Tecnología Agropecuaria). (2009). *Cobertura del suelo de la República Argentina. Año 2006–2009* [Online]. Available: http://inta.gob.ar/documentos/cobertura-del-suelo-de-la-republica-argentina.-ano-2006-2007-lccs-fao/
[9] V. C. Pántano and O. C. Penalba, "Respuesta de la situación hídrica del suelo a la variabilidad temporal de la precipitación," in *Proc. XI Congreso Argentino de Meteorología (CONGREMET XI)*, Mendoza, Argentina, 2012, 12 pp.
[10] V. Y. Bohn, M. C. Piccolo, and G. M. E. Perillo, "Análisis de los períodos secos y húmedos en el sudoeste de la provincia de Buenos Aires (Argentina)," *Revista de Climatología*, vol. 11, pp. 31–43, 2011.
[11] H. Rui. (2012). *Document for the Global Land Data Assimilation System Version 2 (GLDAS-2) Products* [Online]. Available: http://disc.sci.gsfc.nasa.gov/hydrology/documentation
[12] H. Rui and H. Beaudoing. (2015). *README Document for Global Land Data Assimilation System Version 2 (GLDAS-2) Products* [Online]. Available: http://hydro1.sci.gsfc.nasa.gov/data/s4pa/GLDAS/README.GLDAS2.pdf
[13] J. Sheffield, G. Goteti, and E. F. Wood, "Development of a 50-yr high-resolution global dataset of meteorological forcings for land surface modeling," *J. Clim.*, vol. 19, no. 13, pp. 3088–3111, 2006.
[14] [Online]. Available: http://www.conae.gob.ar
[15] A. Stoffelen, "Toward the true near-surface wind speed: Error modeling and calibration using triple collocation," *J. Geophys. Res.*, vol. 103, no. C4, pp. 7755–7766, 1998.
[16] C. Draper, R. Reichle, R. de Jeu, V. Naeimi, R. Parinussa, and W. Wagner, "Estimating root mean square errors in remotely soil moisture over continental scale domains," *Remote Sens. Environ.*, vol. 137, pp. 288–298, 2013.
[17] T. B. McKee, N. J. Doesken, and J. Kleist, "The relationship of drought frequency and duration to time scales," in *Proc. 8th Conf. Appl. Climatology*, 1993, pp. 179–184.
[18] M. J. Hayes, M. D. Svoboda, D. A. Wilhite, and O. V. Vanyarkho, "Monitoring the 1996 drought using the standardized precipitation index," *BAMS*, vol. 80, no. 3, pp. 429–438, 1999.
[19] C. M. Matsudo and P. V. Salio, "Severe weather reports and proximity to deep convection over Northern Argentina," *Atmos. Res.*, vol. 100, no. 4, pp. 523–537, Jun. 2011 [Online]. Available: http://dx.doi.org/10.1016/j.atmosres.2010.11.004

Francisco Grings received the Ph.D. degree in physics from the University of Buenos Aires, Buenos Aires, Argentina, in 2008.

He is a Physicist and a Research Member with the Instituto de Astronomía y Física del Espacio (IAFE), Consejo Nacional de Investigaciones Científicas y Técnicas (CONICET), Buenos Aires, Argentina. He is responsible for electromagnetic modeling within IAFE's Remote Sensing group. He is leading an Observing System Simulation Experiment (OSSE) project at IAFE. His research interests include time-series Bayesian retrieval of remotely sensed data.

Cintia A. Bruscantini is an electronic engineer currently pursuing the Ph.D. degree in observing systems simulations at the Instituto de Astronomía y Física del Espacio (IAFE), Buenos Aires, Argentina.

She has been working on developing an Observing System Simulation Experiment (OSSE) for the Aquarius soil moisture product. She is collaborating with the National Commission on Space Activities (CONAE), Buenos Aires, Argentina, for the calibration of the microwave radiometer (MWR) onboard the Aquarius/SAC-D. Her research interests include OSSEs and instrument prototype developments.

Ezequiel Smucler is pursuing the Ph.D. degree in mathematics at the University of Buenos Aires, Buenos Aires, Argentina.

His research interests include robust regression for high-dimensional data.

Federico Carballo is currently pursuing the Graduate degree in geology at the University of Buenos Aires, Buenos Aires, Argentina.

Currently, he is a Research Fellow with the Meteorology Department, Servicio de Hidrografía Naval (SHN), Buenos Aires, Argentina. From 2011 to 2015, he worked as an Assistant Student with the Instituto de Astronomía y Física del Espacio (IAFE), Buenos Aires, Argentina. At present, he is responsible of the image processing and construction of database for GIS in the department of meteorology (SHN). His research interests include the analysis of sea ice concentration and soil moisture.

María Eugenia Dillon received the Graduate degree in atmospheric sciences from the University of Buenos Aires (UBA), Buenos Aires, Argentina, in 2012.

She has a Ph.D. Fellowship from the Consejo Nacional de Investigaciones Científicas y Técnicas (CONICET), National Meteorological Service of Argentina, Buenos Aires, Argentina. Currently, she is a Teaching Assistant Interim with the Atmospheric and Oceanic Sciences Department, UBA. Her research interests include regional data assimilation using numerical weather prediction models, mesoscale modeling, and the study of soil moisture variability impacts on regional forecasts.

Estela Angela Collini received the Doctor degree in atmospheric sciences from the University of Buenos Aires (UBA), Buenos Aires, Argentina, in 2009.

She is the Director of Projects with Naval Hydrographic Service/National Meteorological Service, Buenos Aires, Argentina, focused on NWP modeling. Her research interests include volcanic ash dispersion, transport and deposition forecast modeling, studies on the soil moisture variability impacts on regional forecasts, NWP models evaluation, and NWP data assimilation.

Mercedes Salvia received the Ph.D. degree in biology from the University of Buenos Aires, Buenos Aires, Argentina, in 2010.

Since 2012, she has been a Biologist Researcher with Consejo Nacional de Investigaciones Científicas y Técnicas (CONICET), Buenos Aires, Argentina, and with the Quantitative Remote Sensing Group, Instituto de Astronomía y Física del Espacio (IAFE), Buenos Aires, Argentina, working in microwave remote sensing for hydrological applications in La Plata Basin.

Haydee Karszenbaum is a physicist and research member of Consejo Nacional de Investigaciones Científicas y Técnicas (CONICET), a remote sensing specialist, and Director of the Remote Sensing Group at the Instituto de Astronomía y Física del Espacio (IAFE), Buenos Aires, Argentina. Since 1997, she is dedicated to microwave remote sensing. She is currently the PI of national projects and of Space Agencies AO projects.